76th International Astronautical Congress (IAC), Sydney, Australia, 29 September - 03 October 2025.

IAC–25–IAC-25,C3,2,12,x101968

Estimating the Potential Impact of SPSs on Space Environment Stability via Stochastic Network Analysis

Pietro De Marchi[a*], Yirui Wang[b], Massimiliano Vasile[c], James Campbell[d], Josh Ferrier[e], Niranjana Gopalakrishnan[f]

[a] *University of Strathclyde, Glasgow, United Kingdom, pietro.de-marchi@strath.ac.uk*
[b] *University of Strathclyde, Glasgow, United Kingdom, massimiliano.vasile@strath.ac.uk*
[c] *University of Strathclyde, Glasgow, United Kingdom, yirui.wang@strath.ac.uk*
[d] *Brunel University of London, London, UK, james.campbell@brunel.ac.uk*
[e] *University of Strathclyde, Glasgow, United Kingdom, josh.ferrier.2021@uni.strath.ac.uk*
[f] *University of Strathclyde, Glasgow, United Kingdom, niranjana.gopalakrishnan.2021@uni.strath.ac.uk*
[*] *Corresponding author*

Abstract

In recent decades, numerous studies have addressed various aspects of Solar Power Satellite (SPS) missions, with particular focus on assembly optimization, energy transmission, decommissioning, and mission design. Despite the potential implications, the literature provides limited systematic frameworks for assessing the short- and long-term effects of SPS systems on the space environment in terms of collision risk and debris generation. The introduction of large-area structures with long operational lifetimes and complex end-of-life scenarios may threaten the already fragile equilibrium of the orbital environment. This study proposes a novel framework for evaluating the long-term debris-related environmental impact of SPS systems, with a focus on how potential collisions may affect the stability of different orbital regions depending on mission parameters such as lifetime, manoeuvrability, and operational orbit. The analysis is based on NESSY (NEtwork model for Space SustainabilitY), a space environment evolutionary model based on network theory developed at the University of Strathclyde. This research enhances the NESSY framework to account specifically for SPSs by introducing a tailored collision risk and breakup model that distinguishes between various components, enabling more accurate estimations of both major and minor debris production. Furthermore, localized connectivity and diffusivity indices are developed to better capture the regional impact of collisions—an improvement over existing models that primarily evaluate global effects and may thus underestimate the localized consequences of SPS collisions. In conclusion, this approach provides a more detailed and region-specific assessment of the debris risks posed by SPS systems, supporting more informed design and policy decisions. By capturing both local and global impacts of potential collisions, it enhances long-term space sustainability and helps prevent cascading debris scenarios that could threaten future space operations.

Nomenclature

a	fragments characteristic length $[m]$
α^n	global connectivity index [-]
β_i	impact angle $[^\circ]$
D_i	impactor largest diameter $[m]$
Δv	collision velocity increment $[\frac{km}{s}]$
η	per–hop transmission factor [-]
J	impact impulse (per link) $[Ns]$
m_i	impactor mass $[kg]$
$p()$	probability or likelihood [-]
R_s	local connectivity [-]
τ	nodes collision rate $[\frac{1}{s}]$
T_t	target thickness $[m]$
v_i	impactor speed $[m/s]$

Acronyms/Abbreviations

LEO	Low Earth Orbit
MOID	Minimum Orbit Intersection Distance
NASA SBM	NASA Standard Breakup Model
PDF	Probability Density Function
SPS	Solar Power Satellite
SBSP	Space-Based Solar Power

1. Introduction

Space-Based Solar Power (SBSP) has been investigated since the 1970s, with early studies driven by the promise of delivering large amounts of clean energy from orbit to Earth. In recent years, the growing urgency of sustainable energy production has renewed interest in these concepts, moving research closer to potential demonstration and commercial missions. Despite this progress, only

a limited number of architectures have been investigated in detail, mainly due to the technological complexity and high costs involved.

Among the most significant proposals in Geostationary Orbit (GEO) is the SPS-ALPHA concept by NASA, designed to deliver approximately 1 GW of power to Earth [1]. A related GEO architecture is CASSIOPeiA (Constant Aperture, Solid-State, Integrated, Orbital Phased Array), developed from the earlier HESPeruS concept [2, 3], with an intended capacity of more than 1 GW. Both architectures rely on very large phased-array reflectors to concentrate solar energy and transmit it to the ground. The first on-orbit technology demonstration, the Space Solar Power Demonstrator (SSPD-1), was launched by Caltech in 2023 [4], marking a key milestone in the field.

An alternative approach, recently under study by ESA and Thales Alenia Space, is the SOLARIS project [5]. This concept envisions a constellation of large, ultra-thin reflectors deployed in Low Earth Orbit (LEO). Each reflector consists of a composite membrane of about 1 km in diameter and only 4–8 μm thickness, supported by a truss ring and a central mast approximately 564 m in length. The system is designed for a dawn-dusk Sun-synchronous orbit at about 890 km altitude. By contrast, the CASSIOPeiA design for GEO features a vertical structure about 3 km in height, with reflectors 2 km in diameter.

While mission studies for these systems have addressed aspects such as assembly, power transfer, orbital insertion, and operational control, much less attention has been devoted to their interaction with the orbital environment. In particular, the collision risk and fragmentation potential of such unprecedentedly large and thin structures remain poorly understood. The challenge is especially critical in LEO, where object density is high and the geometry of thin reflector membranes makes traditional debris modelling approaches inadequate. In GEO, although collision probabilities are lower, the sheer size of concepts such as CASSIOPeiA requires dedicated risk assessment methodologies. The complexity of these structures, which is the reason for the need for such peculiar development, is well represented by the SPS-Alpha concept pictured in Figure 1.

The objective of this paper is to fill this gap by introducing a framework to estimate the environmental impact of SPS systems on the orbital environment in terms of collision risk, debris production, and long-term consequences. The methodology is applied to the ESA reflector concept in LEO and the CASSIOPeiA architecture in GEO, but it can be extended to other SPS designs. This framework is integrated into the NESSY (NEtwork model for Space SustainabilitY) evolutionary model, enabling both global and regional assessments of SPS-related debris risk, and supporting the development of sustainable space policies and mission designs.

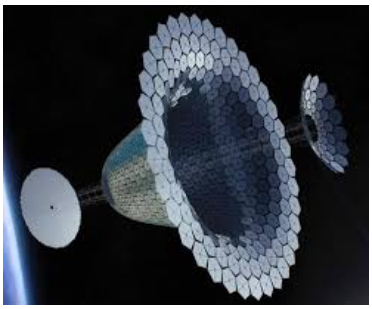

Fig. 1. NASA SPS-Alpha concept representation [credits NASA].

2. Methods for the quantification of the SPSs' impact on the space environment

As previously anticipated, several challenges arise in developing an ad-hoc pipeline for quantifying the impact of SPSs on the space environment. Based on these challenges, we identified the main objectives for the proposed pipeline: (i) the capability to accurately simulate the fragmentation of unconventional structural geometries that are not typically addressed by standard breakup models; (ii) the ability to forecast the evolution of the space environment in the presence of SPS structures; and (iii) the definition of metrics to quantify collision risk within specific orbital regions due to SPSs.

The following sections describe the main methods developed to address these points. The following approaches are all part of the same environment, which is based on the NESSY network model, allowing the forecast of the space environment and its inspection over time. The components of this pipeline ar the following: (i) an evolutionary model to estimate the space environment changes in time, (ii) an estimator of collision likelihood for the different macro components of an SPS, and (iii) a breakup model to adequately account for fragmentations due to impacts tailored for SPSs.

2.1 NESSY: evolutionary model

NESSY is the evolutionary algorithm developed at the Aerospace Centre of Excellence at the University of Strathclyde, allowing us to compute the evolution of the space environment in time, starting from an initial population and eventually including new mission launches. NESSY modelling is reported in detail in [6], while the main modelling aspects are briefly described here. NESSY's main

novelty is its core algorithm based on the network theory, which better allows for inspecting the spreading of the events' effects through the orbital regions. NESSY's network considers the repartition of the physical space around Earth in "nodes", each node is characterised by a range of inclination and altitude. Space objects are grouped into four classes: Payloads (P), Upper-Stages (U), Fragments (F) and Non-Maneuvrable (N) objects. The resident population used in NESSY is extracted for LEO from SatCat TLEs [7] and ESA DISCOS [8]; while for GEO, just from ESA DISCOS data. The F classt includes objects bigger than 1 mm, considering objects with a bigger dimension higher than 10 cm as single objects, while between 10 cm and 1 mm are treated as spatial densities as defined also in ESA Master[9]. This model has been adapted to welcome the class of SPS, mainly because its physical characteristics are too different from those of the other classes. The environment evolution is considered in this paperwork only for the LEO (altitudes up to 2000 km) and GEO (both GEO and EGO are considered, as defined in ESA's annual report [10]) regimes, not considering orbits crossing both regions or transfer orbits (like GTOs) yet. In NESSY, the collision rate between objects in nodes is computed in the following way (described in detail in Reference [11]):

$$\tau_{S_i S_j} = \rho_{S_i} \rho_{S_j} \sigma_{S_i S_j} \Delta v_l U_l \qquad [1]$$

where ρ_S is the spatial density of node S defined by the fraction of number of objects n_S and volume V_S. Assuming dr is the shell thickness and r is the radius at the bottom of the shell, the volume of a node V_S can be calculated by the volume of a sphere minus the volume of two spherical cones. While Δv_l is the relative collision velocity between two colliding objects in crossing nodes and U_l is the volume of the sphere where objects intersect. Once a collision with the SPS is identified, the part of the structure impacted is selected through the probability values for each component derived from the likelihood analysis. While for all the objects in NESSY the NASA SBM is employed, SPS's collisions are treated using the custom breakup model described in the following section, an ad-hoc formulation defined to improve the fragmentation description for such structures. Different from the other classes the SPS class (S) is defined in NESSY as a manoeuvrable object capable of station-keeping and collision avoidance manoeuvres. In the end-of-life phase for the LEO scenario, it is reasonable to think that a maximum drag configuration could be considered, while for the rest of the time, it is oriented to be able to minimize the drag and optimize the orientation to the Sun. In the GEO scenario, instead, the SPS at the end-of-life is moved to a graveyard orbit or transferred far from the Earth's sphere of influence to avoid possible collisions.

While for LEO environment evolution a lot of literature shows methods to estimate the evolution of the environment in time, for the GEO region, just a few studies have been presented. For the LEO simulation NESSY has been validated as compared with MOCAT-MC developed by MIT [12] (full analysis in [6]). All main forecast analyses in GEO focus more on the estimate of the collision risk, like in [13], presenting an analysis for the collision likelihood in GEO, or works like [14] and [15] studying collision hazards with respect to debris in GEO instead.

As indicated before in the evolutionary simulations also small fragments (diameter between 10 cm and 1 mm) are considered in a dedicated node of NESSY. Many studies have inspected methods for small fragments debris densities propagation in time, usually treated considering the analogy of debris clouds with the gas theory (as done in References [16], [17], [18], [19]). In the present model, a simplified and approximated approach is considered to minimize the computational cost and better adapt to the network structure, as NESSY is a low-fidelity simulator. The number of fragments for each node can be recovered from Master densities, considering the altitude shells discretisation provided by Master itself (100 altitude bins between 200 and 2000 km altitude), associated also with the objects' diameter. At the beginning of the simulation, each shell is associated with an average initial altitude, depending on the discretisation itself (average of the altitudes in the range provided by Master). The altitude derived is used for the analytical propagation in NESSY (for LEO or GEO perturbations), combined with the object size provided by Master distributions. Some tools have been developed in the past to estimate collisions with small fragments in time, but their analysis is usually limited to medium-sized objects. For example, ESA DRAMA is limited to missions' maximum cross-sectional area of 1000 m^2.

2.2 SPSs collision probability definition

Once a collision with SPS is detected inside NESSY, the impacted SPS components must be selected, since different parts would lead to very different fragmentation patterns.

The part selected is chosen via the computation of collision likelihood for the SPS. This combined with the mass threshold analysis allows us to estimate the encountered severity for the mission. The likelihood is the probability of finding a background population object at a distance smaller than the MOID (Minimum Orbital Intersection Distance) threshold considered (λ). This probability is derived through an intersection of distributions method [20].

In the next formula, p is the likelihood for a satellite having MOIDs with the background population within a certain threshold distance λ:

$$p(\text{MOID} < \lambda) = \frac{N_{\text{sat}} N_{\text{bkgd}}}{N_I} \sum_{i=1}^{N_I} \left(p(\mathbf{x}_{\text{sat}}^{(i)}) p(\mathbf{x}_{\text{bkgd}}^{(i)}) \right) \cdot \left(\text{MOID}^{(i)} < \lambda \right) V_{\text{sat}} V_{\text{bkgd}} \quad [2]$$

where N_I is the number of samples of the distribution used to integrate, $\mathbf{x}_{\text{sat}}^{(i)}$ and $\mathbf{x}_{\text{bkgd}}^{(i)}$ are samples from the orbital parameters of the mission of interest and background population (composed by DELTA [21] and MASTER [22] objects at the end of 2023), respectively, $(MOID^{(i)} < \lambda)$ is 1 when the MOID is less than the threshold and 0 otherwise, and V_{sat} (is the volume of a hyperellipsoid with radius 6σ in each direction) and V_{bkgd} are the volumes of orbital parameters over which the distributions are sampled. The threshold λ can instead be derived from the maximum probability of collision that can be accepted for a mission. $p(\mathbf{x}_{\text{sat}}^{(i)})$ for the mission considered is derived considering a series of Probability Density Functions (PDF). For a single simple satellite, this is done with a combination of three normal distributions (considering an ellipsoid around the object as the uncertainty volume). In the SPS's case, PDFs are different for each sub-component, to optimally account for the uncertainty about their position knowledge. Distributions are considered on a range of values around the local RTN reference frame centred in the centre of mass of the satellite. The same approach can be adapted to any other mission with similar characteristics.

Figures 2, 3, 4 show the Probability Density Functions defined for the reflector components. PDFs are obtained through a range of values sampling the given distribution, characterised by a certain mean and covariance. Distributions are modelled to optimally represent the shape of the reflector components with respect to its local body frame. In the figures, the blue curve stands for the probability distribution over the three coordinates (in km) and the combined one for the reflector (radius of 500 m); while the red curve (the baseline) is the equivalent normal distribution using the same sampling on the RTN parameters (when only blue is visible is because of superposition).

The reflector attitude considered in those plots corresponds to the operational configuration, so with the main face in the plane of the orbital velocity; different attitudes can be also considered with this method. Three different distributions are considered: normal, normal combined with uniform and two-normal combination. The normal combined to uniform distribution is instead used to model the main face of the membrane or the bigger dimension of the central body. Instead, combining two nominal distributions accounts for the ring shape.

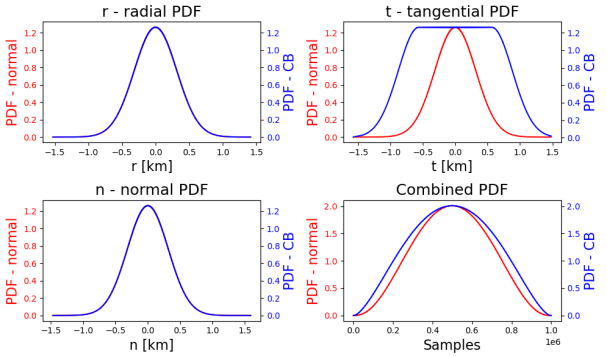

Fig. 2. LEO reflector's central body (CB) PDF. The radius of the reflector is 500 m.

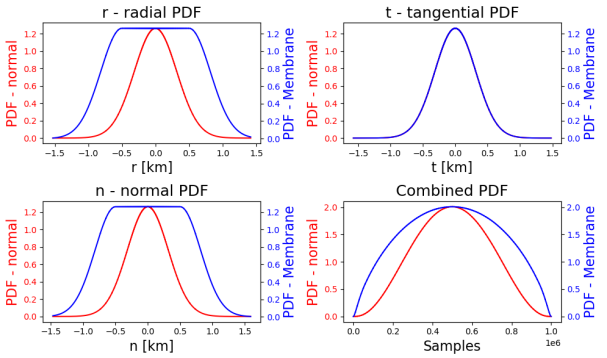

Fig. 3. LEO reflector's membrane PDF. The radius of the reflector is 500 m.

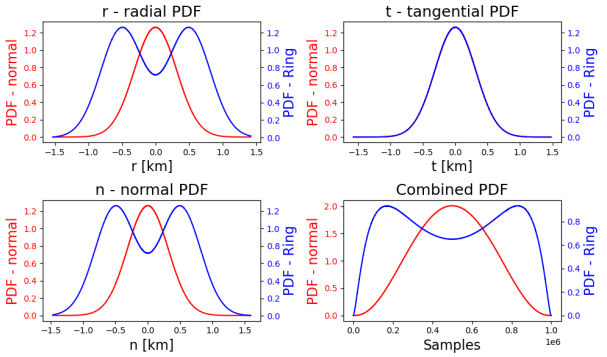

Fig. 4. LEO reflector's ring PDF. The radius of the reflector is 500 m.

2.3 SPSs custom breakup model

A custom breakup model has been developed to better catch the behaviour of breakups involving SPS structures. The scheme of the fragmentation pipeline is presented in Figure 5. This pipeline (previously presented in [23] and detailed in [24]) is mainly composed of two models: one addressing collisions with large uniform structure of the SPS (lower branch of the pipeline in the figure), and the other to model the effects of impacts on more complex structures composed of interconnected elements (upper branch of the pipeline). The first approach refers to any impactor striking large solid components (comparable to plates much larger than the impactor's dimensions) of the SPS, or components that can be modelled similarly. In this first approach, a distinction is made between impactors larger and smaller than 1 m in diameter. For smaller impactors, empirical fragmentation cumulative laws (of the type $N(>a)$), interpolated for missing data. Empirical laws derived from experimental data are of the shape, where N is the number of fragments larger than a certain dimension (characteristic length):

$$N(>a) \;=\; C_{\text{eff}}\,(M_{\text{eq}})^{\alpha_{\text{eff}}}\,a^{-\gamma_{\text{eff}}}, \qquad [3]$$

For larger impactors, an NSBM-like fragments adapted distribution law is employed, because of the lack of available empirical data. Main sources employed for this development are: Piekutowski [25], Verma and Dhote [26], and Nishida [27, 28]. Larger-scale campaigns such as SOCIT [29] and DebriSat [30] also provide reference data. In these scenarios, the pure standard NSBM is insufficient; for instance, when a fragment impacts the entire reflector of the CASSIOPEIA SPS, a more detailed and localised analysis is required to accurately model the fragmentation pattern. The other branch of the pipeline handles impacts with reticular SPS structures, which are common in these mission concepts, such as reticular trusses or large panel-based assemblies. This part allows for defining the separation of main elements and fragmentation mass due to the transfer of impact energy. The approach is based on Paluszny et al. [31] for fracture modelling in finite-discrete element structures, combined with empirical data such as Wittel experiments [32]. The separation of the main components (called also "primitives", the panels or trusses) happens when all the joints around it are broken. On the other side a joint is defined broken as a consequence of an impact when the J (impulse, $[Ns]$) threshold for that material and type of joint is exceeded. The impulse is propagated through the reticular structure per graph hop, and can be modelled as (J is the impact impulse):

$$J_{k+1} = \eta\, J_k, \qquad 0 \le \eta \le 1. \qquad [4]$$

The main materials considered for SPS structures are aluminium (for large panels and structural components), carbon fibre (for most reticular structures and membranes), and honeycomb (for certain panel types). The current model can provide fragmentation patterns with a minimum dimension of 1 mm.

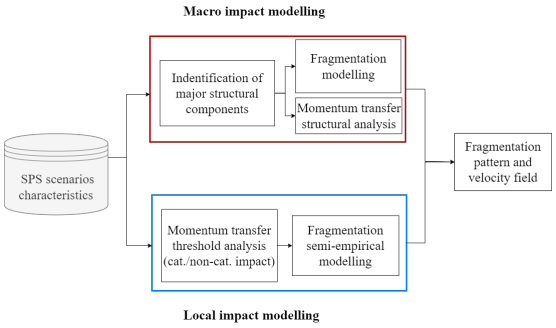

Fig. 5. SPECS fragmentation model pipeline.

2.4 Network analysis metrics

The network architecture allows for inspection of the evolution of the regions of the space environment, based on the interaction of nodes. The main phenomenon we want to monitor via the network analysis is the growth of the space population in the different regions of space because of the presence of certain objects. If a population grows constantly in time in a certain region, this could be defined as a divergence of the local environment that could also lead in the future to a more extensive divergence, or remain localise. This is one of the main goals of the network analysis process. Among the different indices developed so far in NESSY, two main metrics are very useful for the assessment of a space mission's presence on the space environment: the *global* and *local connectivity*. In order to define these metrics it is important to stress the network nature of the NESSY model. Each node of NESSY is a space region (range of inclination and altitude) containing objects of the same type (e.g. payloads). While the site is the region of space containing any type of object located in that region, or the sum of all nodes of the same region. Each node or site is connected by "links" or fluxes of objects moving through nodes, which could be due to the decay (in this case, the flux of objects could be of fragments or also satellites decaying through shells) or collisions (in this case, instead of fragments derived from fragmentation events).

Local connectivity, also defined as R_s, is defined, for a certain site j, as:

$$R_s = \frac{\sum_j^n \rho_{ij}^{\cdot}}{n} \qquad [5]$$

accounting for the local maximum probability of an event spreading around its neighbourhoods. ρ is the maximum bottleneck value from site i to site j.

The global connectivity, defined also as α^n, can be expressed with the following equation:

$$\alpha^n = \frac{1}{n}\sum_{i}^{n}\left(\frac{\sum_j^n \rho_{ij}^{\cdot}}{n}\right) \quad [6]$$

where index i spans over all the sites of the network and j covers all the linked sites to the one considered.

The global connectivity can be understood as the probability that if a collision event happens in the space environment, it spreads in all regions, also affecting them. While local connectivity tries to quantify the same effect, but just considers a single site of the space environment with respect to its neighbourhoods.

3. Test cases and Results

In this section, some test cases are selected to show the behaviour of the tool. A couple of impact examples are selected to visualise the fragmentation characteristics, as reported in Table 1: one local fragmentation and a primitives structure fragmentation for a reticular ring truss structure. In the table, β_i stands for the impact angle with respect to the normal direction.

Table 1. Test cases for impact analysis.

Impact test cases			
Test case	Pipeline regime	Impactor	Target
Test-1	Local $D_i < 1m$	D_i = 0.4m v_i = 10$\frac{km}{s}$ Al6061	T_t = 10mm Al6061 β_i = 0°
Test-2	Modular structure	D_i = 0.5m v_i = 10$\frac{km}{s}$ Al6061	3D ring CFRP $N_e = 300$

Furthermore, a NESSY propagation test is considered, placing the ESA reflector SPS in LEO region in three different orbits, and propagating the space environment for 50 years starting from the 2023 pace resident population. The NESSY model is stochastic, so it has been run for 200 Monte Carlo runs to produce the propagation results. Ultimately, the connectivity for these same NESSY test cases is computed to assess the effect of the SPS structure in LEO orbit.

3.1 Test-1: local fragmentation, D <1 m

The first test inspects the case of impact between a spherical fragment of 400 mm diameter and an SPS panel 10 mm thick, both of aluminium. The impact speed is 10 $\frac{km}{s}$, perfectly normal to the plate plane. Figure 6 reports the Voronoi-based fragmentation pattern sizes based on the interpolated empirical law for the impactor-target couple. The empirical cumulative law used is plotted on the right side (yellow) with its truncated form (blue, to meet the maximum fragment size constraint), together with the Voronoi fragments distribution (red). Minimum dimension considered in this test is 1 cm. Voronoi fragments follow the empirical law with a slight tendency to overestimate for higher dimensions.

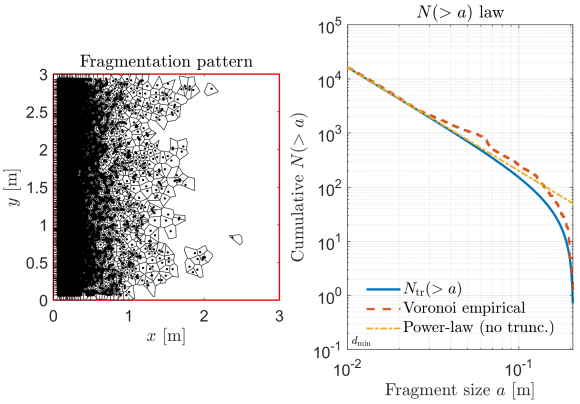

Fig. 6. Test-1 Voronoi pattern (on the left) and $N(>a)$ cumulative law comparison between interpolated empirical N law against Voronoi generated fragments (on the right).

Figure 7 instead shows the distribution of Voronoi-based fragment sizes (blue bars) against the NASA SBM distribution for the same test case. NASA SBM provides slightly higher values of area-to-mass ratio with respect to the Voronoi approach, as also observed in Francesconi et al. [33]. While the Δv-to-area ratio is quite in agreement with the NASA SBM distribution. The fragmentation model then also allows to compute the orbital parameters for each parameter, derived from the Δv distribution estimated for each fragment (more details in [24]).

3.2 Test-2: primitives modelling

In this section Test-2 results analysis is reported. Table 2 provides more details about the reticular truss structure impacted. The impactor is considered again a sphere of aluminium of 0.5 m diameter and impacting at 10 $\frac{km}{s}$. This example can be considered as a good representation of the ESA LEO reflector concept external ring (see Thales report [5]).

Figure 8 represents the entire ring 3D, seen from the top: trusses are represented as grey lines connected by

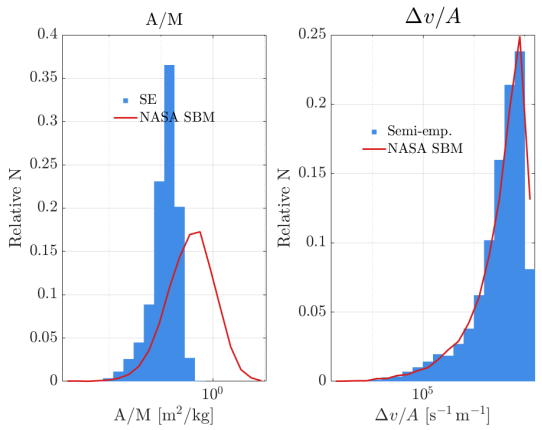

Fig. 7. Test-1 Voronoi-based (blue bars) vs NASA SBM (red curve) fragments distributions: area-to-mass ratio (left) and Δv-to-area ratio (on the right). Distribution reported for the number of fragments normalised to the total number of fragments generated.

grey dots (intact joints). In Figure 8 and Figure 9, broken links because of the impact are plotted as red dots, while secondary fragmented trusses are plotted in violet. The impact point (the point where the impactor hits the structure) is instead indicated with a blue dot in these figures (except for Figure 10 where it is red). Figure 10 shows instead the impulse J values for all the joint points around the impacted region of the truss structure, together with J threshold defined by the tool reported on the colorbar.

Table 2. Reticular structure definition. Nomenclature: h=height of the trusses, t=thickness of trusses, D_{out}=external diameter of trusses, J_{thr}=threshold impulse for trusses separation.

Component	Number	Properties
Trusses	1330	h = 1 m t = 5 mm D_{out} = 5 cm CFRP
Joints	380	type = bolted $J_{thr} = 143\ Ns$

The impact imposes a fracture of 44 joints of the structure and fragmentation of 46 trusses (total fragmented mass 22.08 kg). Impulse due to the impact decays inside the structure by the empirical law described in the previous section [24]. The model can estimate the size distribution of fragments from the considered mass with the same approach presented for local fragmentation, distributing mass and Δv to each fragment. The same approach can be employed to study elements separation and fragmentation on other types of geometries: 2D truss structures, 2D panel structures and 3D truss structures with different shapes.

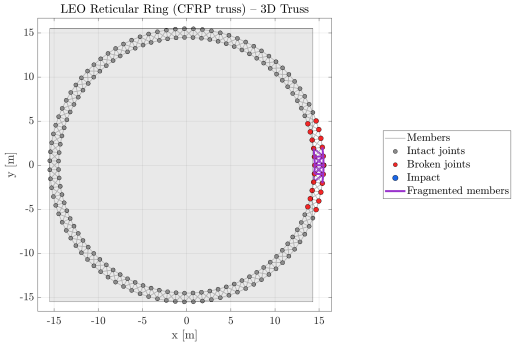

Fig. 8. Test-2 3D truss structure top view via primitives modelling: broken joints are plotted with red dots, while intact joints are in grey, and fragmented trusses are in violet.

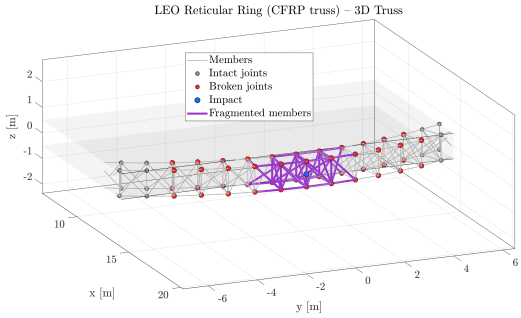

Fig. 9. Test-2 3D truss structure lateral view via primitives modelling: broken joints are plotted with red dots, while intact joints are in grey, and fragmented trusses in violet.

3.3 NESSY propagation test cases

The breakup model described so far has been integrated into the NESSY evolutionary model to examine the long-term effects of the SPSs' presence in orbit. The SPS mission considered here is the ESA reflector concept, placed in three different LEO orbits (h = orbit altitude, inc = orbit inclination): (i) h_1 = 560 km, inc_1 = 97.7°, (ii) h_2 = 890 km, inc_2 = 99°, (iii) h_3 = 1200 km, inc_3 = 100.7°. These tests consider different Sun-Synchronous Orbits for the LEO reflector, whereas current studies have so far only considered the lowest one.

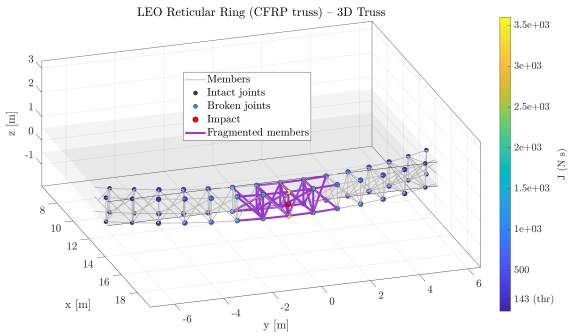

Fig. 10. Test-2 3D truss structure lateral view via primitives modelling: J propagated over joints is plotted with heatmap colours to show its distribution on the structure itself.

Additional details are also provided about the simulation settings for the LEO region. The network discretisation used for the following results is 60° in inclination and 50 km for altitude shells. We assumed a PMD (Post-Mission Disposal) period of 5 years, i.e. a new payload is removed from the environment after 5 years if still active, and a PMD failure rate of 5%. This failure rate results in a proportion of payloads becoming non-manoeuvrable satellites. The success rate of collision avoidance manoeuvres, s_{CAM}, was set to 99.9%. These assumptions are further described in [6]. For the SPS mission, no collision avoidance is considered in this test case in order to assess the worst possible scenario. Furthermore, the SPSs are assumed to have an operational lifetime of 7 years; afterwards, they decay in maximum-drag configuration. The baseline initial population corresponds to the resident objects at the end of 2023 in the LEO regime (below 2200 km altitude): 5471 payloads, 1111 upper stages, 9804 fragments, and 2440 non-manoeuvrable satellites. For the test cases reported here, only objects larger than 10 cm are considered, including all fragments produced by collisions.

Figure 11 shows the average NESSY propagation over 50 years for the baseline population (red) and the different reflector orbits. Figure 12 instead reports the distribution of catastrophic collisions over time. The final population in all three cases is higher than in the baseline scenario. This is also reflected in the collision plot. The highest collision rate (more details in Appendix A) occurs in the case of the reflectors at 560 km. However, since the decay rate in this region is very strong, the resulting population is not the largest. The collision distributions for the 890 and 560 km cases are very close, with the 890 km case ending with the highest population because the reflector remains in the space environment for a longer time.

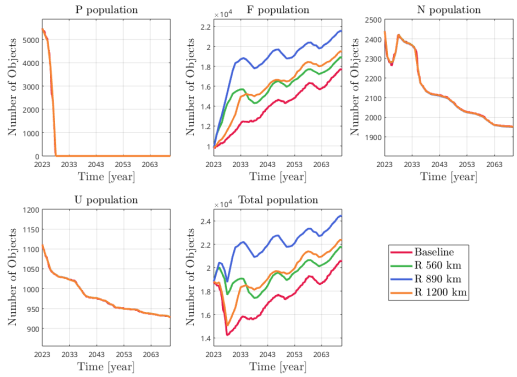

Fig. 11. NESSY population ($d \geq 10\,cm$) propagation over 50 years (average trend over 200 Monte Carlo runs): baseline resident population against 3 reflectors located at different altitudes. NESSY discretisation 60°-50km.

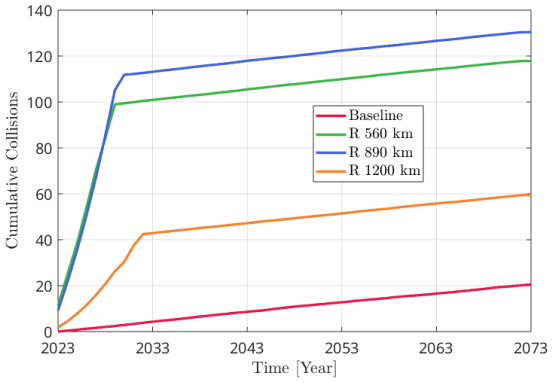

Fig. 12. NESSY cumulative catastrophic collisions over 50 years (average trend over 200 Monte Carlo runs): baseline resident population against 3 reflectors located at different altitudes. NESSY discretisation 60°-50km.

3.4 Connectivity network analysis for reflector tests

Figures 13 and 14 show the evolution of global and local connectivity for the reflector constellations at different orbits compared to the baseline case. Global connectivity shows a net increase, for all tests, during the SPS mission lifetime (first 7 years), then stabilises on the baseline trend once the reflector decays, with values slightly higher than the baseline. This means that the fragments produced by collisions, which are much more frequent with reflectors, still affect the connectivity between sites even after

the SPS has left the environment. The local connectivity plot instead compares the trend for the 800 km test case at the site where the SPS was initially launched, against the baseline for the same site. Local connectivity shows a higher value than in the baseline case, which decreases once the SPS leaves the site; after the SPS has decayed, the trend of local connectivity is decreasing. This difference arises because the presence of the reflector created a series of generally small fragments from larger objects, causing a slight reduction in the collision rate for the site considered. In this case, one could say that the reflector has a kind of "cleaning effect" on the space environment, reducing the size of larger fragments (even if more smaller fragments are produced), and thereby decreasing the collision rate for that specific region.

Comparing the different cases, the 560 km case reports the highest value of α_n, as it has the highest collision rate and lies very close to a densely populated payload region. However, its trend is very close to that of the 890 km case. The 1200 km case instead shows the lowest trend among the SPS cases, with a late peak due to the passage of the SPS through the lower shells after 10 years of simulation.

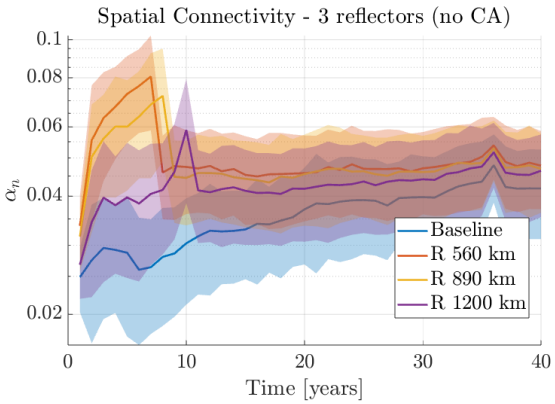

Fig. 13. α_n connectivity evolution for the different test cases along 40 years of simulation. The average trend (solid) is plotted together with the standard deviation (shaded, considering 100 Monte Carlo runs). NESSY network discretisation 60°-50km.

4. Conclusions and next steps

This paper introduces a framework to assess the environmental impact of launching an SPS mission (or a large space structure) into orbit. The major challenges are accounting for the peculiar shapes of large space missions and their specific mission profiles. The present pipeline includes the following approaches:

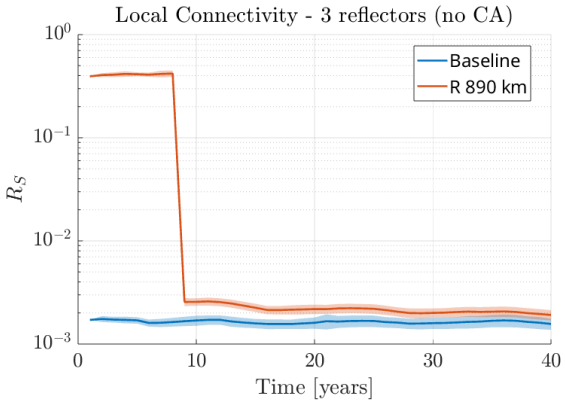

Fig. 14. R_s connectivity evolution for the reflectors at 890 km altitude along 40 years of simulation. The average trend (solid) is plotted together with the standard deviation (shaded, considering 100 Monte Carlo runs). NESSY network discretisation 60°-50km.

- A custom estimate of the collision likelihood for SPSs via PDFs, allowing better accounting for arbitrary shapes
- A new breakup model pipeline, designed to be more suitable for SPS structures' characteristics (shape, materials, types of impact)
- A set of analytics to examine the long-term effects of SPSs in specific orbital regions on the rest of the space environment

The NESSY network model is used to forecast the long-term evolution of the space environment; here just a LEO case is treated, while also GEO is available. This paper reports only the main results to illustrate the capabilities of the tool; further analyses will be presented in future work, more focused on the influence the custom breakup model has on the evolution results with respect to the NSBM.

While the model is capable of covering a wide range of analyses, further improvements are possible. One of the main limitations concerns the breakup model, which does not currently account for the effects of impactor shapes in collision events. Another useful analysis for SPS manufacturers or operators would be ranking orbital regions (depending on the type of SPS selected) in terms of collision risk and environmental impact. To do this, an additional index would be needed, combining the currently available statistics. These analyses will be addressed in future work.

Acknowledgements

This work is partially supported by the ESA-funded project SOLERO - Solar Power Satellite vs the Space Environment, Co-Sponsored Research Agreement No. 4000144200/24/NL/MGu/my.

Appendix A: NESSY collision rate distribution

In order to support the understanding of the connectivity results, the collision rate distribution for the initial timestep (as computed by NESSY) through the LEO shells is reported, considering also the SPS reflectors at 560, 890 and 1200 km. The network discretisation considered in the plots is 60 ° for inclination, and 50 km for altitude shells. This plot reports the pure value of the collision rate computed by the NESSY model, not considering any type of collision avoidance strategy that could mitigate this value. We notice the collision main peaks match the most congested regions of the LEO regions: around 700-800 km altitude and about 1500 km altitude. The highest value of collision rate is for the 560 km case during the first timestep, very close to the 890 km case.

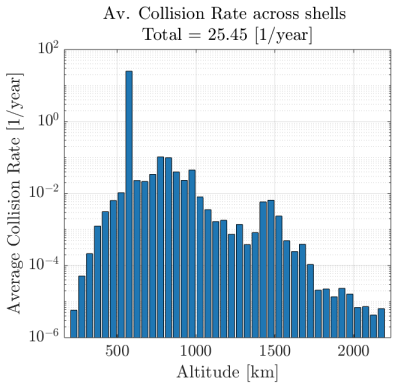

Fig. 15. Collision rate through altitude shells computed at the first simulation timestep for the test case with the three reflectors at 590 km altitude (average of 200 Monte Carlo runs). NESSY discretisation 60°-50km.

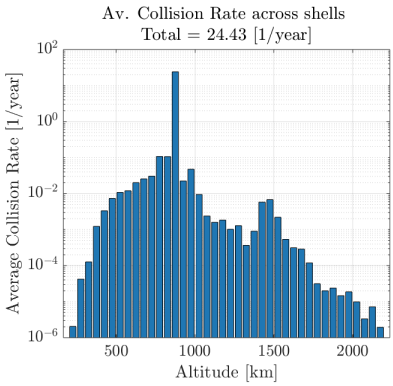

Fig. 16. Collision rate through altitude shells computed at the first simulation timestep for the test case with the three reflectors at 890 km altitude (average of 200 Monte Carlo runs). NESSY discretisation 60°-50km.

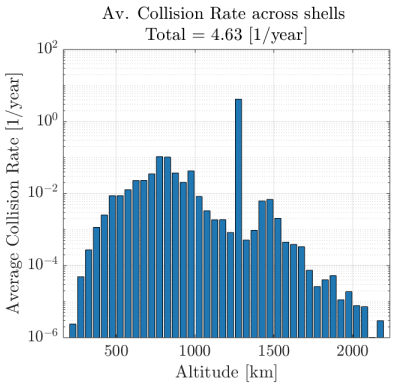

Fig. 17. Collision rate through altitude shells computed at the first simulation timestep for the test case with the three reflectors at 1200 km altitude (average of 200 Monte Carlo runs). NESSY discretisation 60°-50km.

References

[1] J. C. Mankins, "SPS-Alpha: The first practical solar power satellite via arbitrarily large phased array," in *10th International Energy Conversion Engineering Conference*, 2012. DOI: 10.2514/6.2012-3978. [Online]. Available: http://dx.doi.org/10.2514/6.2012-3978.

[2] I. Cash et al., "CASSIOPeiA solar power satellite," in *IEEE International Conference on Wireless for Space and Extreme Environments (WiSEE)*, 2017. [Online]. Available: https://ieeexplore.ieee.org/document/8124908.

[3] C. Mankins, "Sps-alpha: The first practical solar power satellite via arbitrarily large phased array," NASA NIAC Phase 1 Project, Tech. Rep., Sep. 2012. [Online]. Available: https://www.researchgate.net/publication/268573928_SPS-ALPHA_The_First_Practical_Solar_Power_Satellite_via_Arbitrarily_Large_Phased_Array_A_2011-2012_NIAC_Project.

[4] A. Fikes et al., "The Caltech Space Solar Power Demonstration One Mission," in *IEEE*, 2022. [Online]. Available: https://ieeexplore.ieee.org/document/9926883.

[5] SBSP Team Thales Alenia Space, "Pre-phase a system study of a commercial-scale space-based solar power (sbsp) system for terrestrial needs," Tech. Rep., 2023.

[6] Y. Wang, P. De Marchi, and M. Vasile, "A stochastic dynamic network model of the space environment," *Advances in Space Research*, 2025, In Press; Journal pre-proof. Available online 26 Aug 2025, ISSN: 0273-1177. DOI: 10.1016/j.asr.2025.08.051. [Online]. Available: https://www.sciencedirect.com/science/article/pii/S0273117725009408.

[7] L. Stein, *Leo satcom report*, Mar. 2022. [Online]. Available: https://www.primemoverslab.com/resources/ideas/leo-satcom.pdf.

[8] ESA Space Debris Office, *DISCOSweb*, https://discosweb.esoc.esa.int/, Accessed Dec 2024, 2024.

[9] European Space Agency, *Esa master (meteoroid and space debris terrestrial environment reference) tool*, Accessible at: https://www.esa.int, 2024.

[10] ESA Space Debris Office, "ESA's annual space environment report – 2024," European Space Agency, Tech. Rep., 2024. [Online]. Available: https://www.esa.int/Space_Safety/Space_Debris/ESA_Space_Environment_Report_2024.

[11] Y. Wang, C. Wilson, and M. Vasile, "Multi-layer temporal network model of the space environment," in *Proceedings of the American Astronautical Society Meeting*, 2023. [Online]. Available: https://www.researchgate.net/publication/373014561_MULTI-LAYER_TEMPORAL_NETWORK_MODEL_OF_THE_SPACE_ENVIRONMENT.

[12] A. D'Ambrosio, S. Servadio, P. M. Siew, and R. Linares, "Novel source–sink model for space environment evolution with orbit capacity assessment," in *AAS/AIAA Astrodynamics Specialist Conference*, 2022. DOI: 10.2514/1.A35579. [Online]. Available: https://arc.aiaa.org/doi/10.2514/1.A35579.

[13] D. L. Oltrogge, S. Alfano, C. Law, A. Cacioni, and T. S. Kelso, "A comprehensive assessment of collision likelihood in Geosynchronous Earth Orbit," *Acta Astronautica*, vol. 147, pp. 316–345, Jun. 2018, ISSN: 0094-5765. DOI: 10.1016/j.actaastro.2018.03.017. Accessed: Dec. 15, 2024. [Online]. Available: https://www.sciencedirect.com/science/article/pii/S0094576517315011.

[14] P. Shu, M. Zhao, Z.-Y. Li, W. Sun, Y.-Q. Li, and Y.-Z. Luo, "Short-term evolution and risks of debris cloud stemming from collisions in geostationary orbit," *Acta Astronautica*, 2024, Available at: https://www.sciencedirect.com/science/article/pii/S0094576524007653, ISSN: 0094-5765. DOI: 10.1016/j.actaastro.2024.12.016.

[15] H. Zhang, Z. Li, W. Wang, Y. Zhang, and H. Wang, "Geostationary orbital debris collision hazard after a collision," *Aerospace*, vol. 9, no. 5, p. 258, 2022, Available at: https://doi.org/10.3390/aerospace9050258. DOI: 10.3390/aerospace9050258. [Online]. Available: https://doi.org/10.3390/aerospace9050258.

[16] F. Letizia, C. Colombo, and H. G. Lewis, "Analytical model for the propagation of small-debris-object clouds after fragmentations," *Journal of Spacecraft and Rockets*, vol. 52, no. 4, pp. 1108–1122, 2015, Available at: https://doi.org/10.2514/1.G000695. DOI: 10.2514/1.G000695. [Online]. Available: https://doi.org/10.2514/1.G000695.

[17] S. Frey, C. Colombo, and S. Lemmens, "Extension of the king-hele orbit contraction method for accurate, semi-analytical propagation of non-circular orbits," *Advances in Space Research*, vol. 64, no. 1, pp. 1–17, 2019, Available at: https://www.sciencedirect.com/science/article/pii/S0273117719301978, ISSN: 0273-1177. DOI: https://doi.org/10.1016/j.asr.2019.03.016. [Online]. Available: https://www.sciencedirect.com/science/article/pii/S0273117719301978.

[18] C. R. McInnes, "An analytical model for the catastrophic production of orbital debris," *ESA Journal*, vol. 17, no. 4, pp. 293–305, 1993, Available at: https://www.semanticscholar.org/paper/An-Analytical-Model-for-the-Catastrophic-Production-McinnesC/a26586af24aaef59ba0efe9af9ec8484cb4e77ac.

[19] L. Giudici, J. L. Gonzalo, and C. Colombo, "Density-based in-orbit collision risk model valid for any impact geometry," *Acta Astronautica*, vol. 219, pp. 785–803, 2024, Available at: https://doi.org/10.1016/j.actaastro.2024.03.067, ISSN: 0094-5765. DOI: 10.1016/j.actaastro.2024.03.067.

[20] C. Wilson, M. Vasile, J. Feng, K. McNally, A. Anton, and F. Letizia, "Quantifying the induced and encountered risk of space missions: 74th International Astronautical Congress," Available at: https://strathprints.strath.ac.uk/87756/, Oct. 2023.

[21] B. B. Virgili, "DELTA (Debris Environment Long-Term Analysis)," en, *Environmental Science, Engineering*, 2016, Available at: https://indico.esa.int/event/111/contributions/234/attachments/486/531/DELTA_paper.pdf.

[22] V. Braun, A. Horstmann, S. Lemmens, C. Wiedemann, and L. Böttcher, "Recent developments in space debris environment modelling, verification and validation with MASTER," de, 2021. Accessed: May 2, 2024. [Online]. Available: https://conference.sdo.esoc.esa.int/proceedings/sdc8/paper/28.

[23] P. De Marchi, J. Campbell, Y. Wang, and M. Vasile, "The environmental impact of collisions with large space structures: The case of solar power satellites," in *Proceedings of the ESA Space Debris Conference (SDC)*, Presented April 2025, Bonn, Germany, Apr. 2025.

[24] P. D. Marchi, M. Vasile, and J. Campbell, "Specs: A fragmentation estimation framework for solar power satellites and integration into the nessy evolutionary model," in *76th International Astronautical Congress (IAC)*, Copyright © 2025 by the authors. Published by the IAF, with permission and released to the IAF to publish in all forms, Sydney, Australia: International Astronautical Federation (IAF), Sep. 2025. DOI: TODO:addDOIifavailable. [Online]. Available: https://www.iafastro.org/events/iac/iac-2025/.

[25] A. J. Piekutowski and J. Andrew, "Characteristics of debris clouds produced by hypervelocity impact of aluminium spheres with thin aluminum plates," *International Journal of Impact Engineering*, vol. 14, pp. 573–586, 1993. [Online]. Available: https://www.sciencedirect.com/science/article/pii/0734743X9390053A.

[26] P. N. Verma and K. D. Dhote, "Characterising primary fragment in debris cloud formed by hypervelocity impact of spherical stainless steel projectile on thin steel plate," *International Journal of Impact Engineering*, vol. 120, pp. 118–125, Oct. 2018. [Online]. Available: https://www.sciencedirect.com/science/article/pii/S0734743X17311338?via%3Dihub.

[27] M. Nishida, Y. Hiraiwa, K. Hayashi, and S. Hasegawa, "Ejecta size distribution resulting from hypervelocity impact of spherical projectiles on CFRP laminates," *Procedia Engineering*, vol. 58, pp. 533–542, 2013. [Online]. Available: https://www.sciencedirect.com/science/article/pii/S1877705813009673.

[28] M. Nishida, Y. Hiraiwa, K. Hayashi, and S. Hasegawa, "Scaling laws for size distribution of fragments resulting from hypervelocity impacts of aluminum alloy spherical projectiles on thick aluminum alloy targets: Effects of impact velocity and projectile diameter," *International Journal of Impact Engineering*, vol. 109, pp. 400–407, Nov. 2017. [Online]. Available: https://www.sciencedirect.com/science/article/pii/S0734743X16305206.

[29] E. Ausay et al., "A comparison of the socit and debrisat experiments," in *Proceedings of the ESA Space Debris Conference*, 2017. [Online]. Available: https://conference.sdo.esoc.esa.int/proceedings/sdc7/paper/729.

[30] J. Murray and H. Cowardin, "Analysis of the DebriSat fragments and comparison to the NASA standard satellite breakup model," in *First International Orbital Debris Conference*, 2019. [Online]. Available: https://ntrs.nasa.gov/api/citations/20190034081/downloads/20190034081.pdf.

[31] A. Paluszny, X. H. Tang, and R. W. Zimmerman, "Fracture and impulse-based finite–discrete element modeling of fragmentation," *Computational Mechanics*, vol. 52, no. 5, pp. 1071–1084, 2013. DOI: 10.1007/s00466-013-0868-y.

[32] F. K. Wittel, F. Kun, H. J. Herrmann, and B. H. Kröplin, "Mechanisms in impact fragmentation," *arXiv preprint arXiv:1509.00979*, 2015. [Online]. Available: https://arxiv.org/abs/1509.00979.

[33] A. Francesconi et al., "CST: A new semi-empirical tool for simulating spacecraft collisions in orbit," *Acta Astronautica*, vol. 160, pp. 195–205, Jul. 2019. [Online]. Available: https://www.

sciencedirect.com/science/article/pii/
S0094576519302383.